

Energy loss of heavy ions in a plasma target

D. H. H. Hoffmann,* K. Weyrich, and H. Wahl

*Max-Planck-Institut für Quantenoptik, Garching, Federal Republic of Germany
and Gesellschaft für Schwerionenforschung Darmstadt m.b.H., P.O. Box 110552, D-6100 Darmstadt, West Germany*

D. Gardés and R. Bimbot

Institut de Physique Nucléaire, Université Paris Sud, Orsay, France

C. Fleurier

Groupe de Recherches sur l'Energétique des Milieux Ionisés, Université Orleans, France

(Received 8 February 1990)

The energy loss in a plasma target was measured for different heavy-ion species, ranging from ^{40}Ca to ^{238}U at an energy of 1.4 MeV/u. A discharge tube was used to generate a hydrogen plasma with a high degree of ionization and temperatures between 1 and 2 eV. An on-line diagnostic of the plasma was performed to measure the free-electron density and the electron temperature. Compared to neutral hydrogen of the same particle density, the plasma target shows an enhanced stopping power due to the increased energy transfer to the free plasma electrons, and a higher effective charge of the projectiles inside the plasma target. Theoretical predictions based on the Bethe-Bohr-Bloch stopping theory are in good agreement with the experimental results.

I. INTRODUCTION

Intense heavy-ion beams have experienced a steadily increasing attractiveness to deliver the high-power-density deposition of energy on a fusion target, necessary to achieve inertial confinement fusion (ICF), and competing with intense light-ion beams and high-power lasers they offer an especially promising concept for a power reactor. Heavy ions possess most favorable properties to heat small samples of matter to reach regimens of high temperature and density. Due to their high nuclear charge Z they deposit the energy very effectively ($\propto Z^2$) and penetrate deep into the interior of the target, thus constituting an efficient volume heating. Beam-target coupling can then be optimized by choosing the proper combination of ion species and ion energy. Even for multi-terawatt pulses, heavy-ion beams can be transported ballistically and can be focused onto a small target. The production of intense heavy-ion beams benefits from an advanced state of accelerator technology that offers high driver efficiency and high repetition rates.

The new accelerator facilities at GSI-Darmstadt, will be completed in 1990, and high-energy, high-intensity beams will be available for experiments. An experimental program has therefore been launched¹ to utilize the heavy-ion synchrotron [Schwer Ionen synchrotron (SIS)] and the storage ring [Experimentier Speicher ring (ESR)] for the production and focusing of high-power heavy-ion beams. An important issue to assess the merits of intense heavy-ion beams as a driver for ICF pellets is the precise knowledge of energy deposition profiles in a plasma environment, since the design of efficient high-gain targets depends largely on the ability to model the energy-deposition processes in the ablation layer. During the heating process this target layer will be converted to high

temperatures and constitute an environment of highly ionized matter, where the interaction with bound and free electrons will slow down the velocity of the incoming projectile.

While the interaction of heavy ions with bound electrons is sufficiently well understood experimentally as well as theoretically, only a few preliminary experiments have been reported until now that study the energy loss of particles in a plasma target.^{2,3} In a joint collaboration of laboratories in France and Germany we have set out to investigate the energy loss of heavy ions in a plasma target.^{4,5} The hydrogen discharge plasma we used in our experiment provides a plasma target that is well diagnosed, very reproducible, and offers a high degree of ionization (>90%). Thus we are able to investigate the energy-loss phenomena that are due to collisions with free electrons. In this paper we report the results of our measurements for a wide range of heavy ions, and compare these results to theoretical models.

II. EXPERIMENTAL SETUP

The experiment was performed at the 1.4-MeV/u target station of the UNILAC at GSI. In Fig. 1 we present the beamline configuration and a schematic outline of the method of measurement. Important features of the setup are the plasma target, a time-of-flight system to analyze the ion energy, and the deflection of the beam by 15° to enable on-line plasma diagnostic with lasers, collinear to the ion beam.

A. The plasma target

The plasma target is designed as a linear discharge plasma in z-pinch geometry, using hydrogen as target gas to create a hydrogen discharge plasma. This gas is

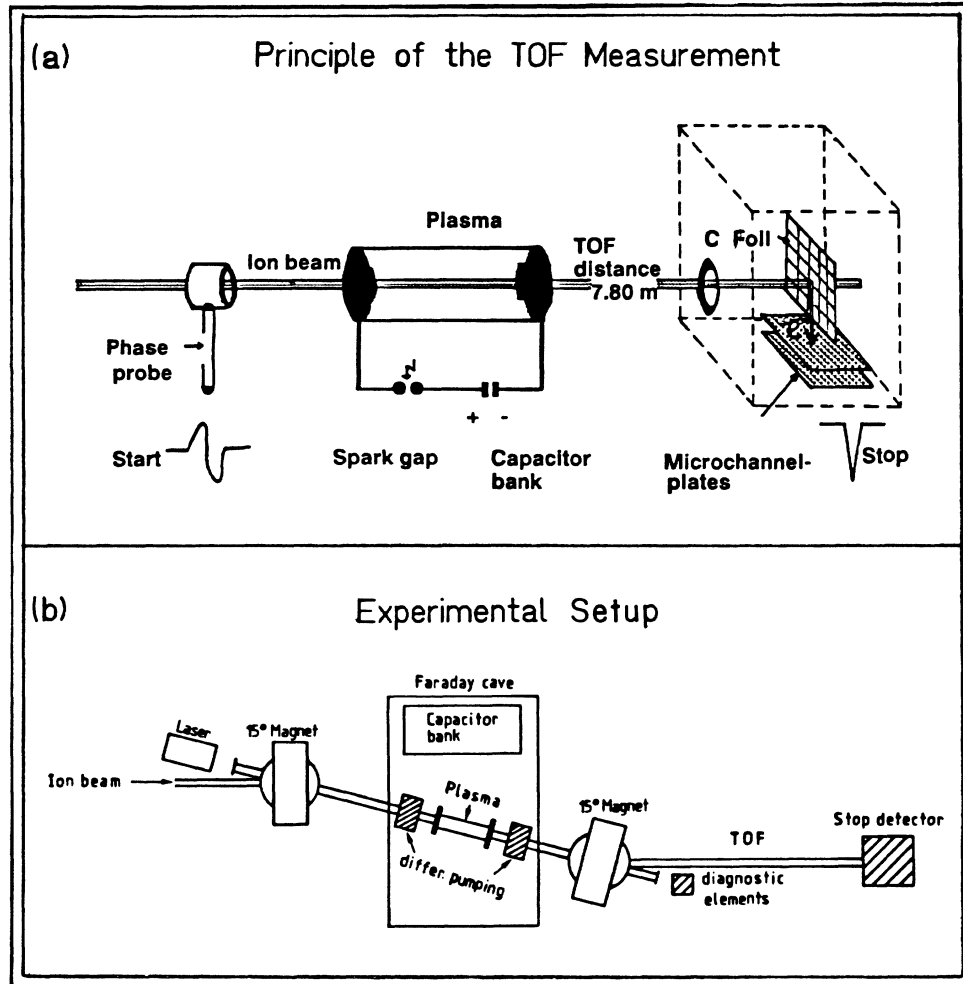


FIG. 1. Schematic setup of the experiment.

confined in a quartz tube of 4 cm in diameter and 36 cm long. At both ends the tube is closed with metal electrodes, which have beam entrance and exit apertures ($\phi=4$ mm). Therefore the gas flow has to be pumped differentially. Using entrance foils instead of pumping the target differentially would destroy the charge state of the incoming ions and increase the energy loss of the ions. In addition to that, entrance foils are likely to be destroyed with every plasma ignition.

The differential pumping system consists of two stages on each side of the plasma, using a powerful roots pump (500 l/min) in the first stage, and in the second using turbomolecular pumps. With an operating pressure of 6 mbar in the target, the final pressure at the second stage is 3×10^{-4} mbar.

The plasma is created by discharging the energy stored in a capacitor bank into the gas volume. This capacitor bank consists of four capacitors ($16.4 \mu\text{F}$ each). Using discharge voltages of 10 to 12 kV, the stored energy ranged between 3.1 and 4.5 kJ. A spark gap is used as a fast switch to release the energy into the gas volume. The reproducibility of the plasma parameters was controlled by monitoring the light output from the plasma, especial-

ly by the emission of the H_{β} line. The transient light signal was detected with a photodiode and displayed on a storage oscilloscope. During the initial phase of the discharge (up to $20 \mu\text{s}$) intensity and shape of the light output varied by more than 10%, but was very stable and reproducible between 20 and $80 \mu\text{s}$ after ignition of the plasma discharge. Since the intensity of the light emission is proportional to the square of the free-electron density n_e , it thus constitutes a suitable signal to monitor the plasma conditions described by the plasma parameters free-electron density n_e and electron temperature T_e .

It was necessary to place the plasma target in a Faraday cave to shield the particle detector and the diagnostic equipment from the rf noise of the discharge.

B. Time-of-flight energy analysis

The energy loss of the heavy ions was measured with a time-of-flight (TOF) system, and the rf microstructure of the ion beam (one beam bunch every 37 ns) was used as a clock. At intervals of 2 min the plasma was fired automatically synchronized with the macrostructure of the beam pulses, which last for approximately 5 ms and have

a repetition frequency of 50 Hz. The 2 min intervals between single shots were used to recharge the capacitors and to allow for time to cool off the plasma quartz tube.

In order to initiate a start pulse for the time-of-flight measurement a signal was derived from the beginning of plasma light emission and brought to coincidence with the pulses from the 27-MHz microstructure of the ion beam in a fast-coincidence unit. Thus the first beam bunch arriving at the detector after the start of the plasma light emission was used to define time zero for the energy-loss measurement. By means of an adjustable delay between the plasma light signal and the 27-MHz signal the start of the time-of-flight measurement could be chosen accordingly.

At the end of the 778-cm-long flight path the stop detector was positioned. Its main component is a thin carbon foil mounted above a stack of two microchannel plates (MCP). Electrons emitted from the carbon foil during the passage of the ion beam are electrostatically deflected onto the MCP's, creating stop signals with a rise time of about 1 ns and an amplitude between 500 mV and 1 V.

The timing signals were sent to a special time-to-digital-converter (TDC), which registered 255 stop pulses following one start pulse.^{6,7} The maximum time resolution for our electronic system was about 1 ns, to be compared with the typical width of the beam bunches of 2 ns. The dead time of the electronic system including the

TDC is 30 ns, and therefore 255 beam bunches arriving at the stop detector in 37-ns intervals give rise to a stop signal. This also means that one measurement covered about 8 μ s, which is approximately one-tenth of the plasma lifetime. One run typically consisted of 100 plasma ignitions. The results were sampled to provide sufficient statistical significance in the time-of-flight spectra.

The actual measurement was performed in three steps as demonstrated in Fig. 2, showing time spectra obtained from the microstructure of the ion beam. The first step is to provide a reference measurement, which we refer to as the vacuum calibration, where the ions have the nominal energy of 1.4 MeV/u. In this case the plasma light signal is simulated. The second step is to fill the quartz tube with the operating pressure of hydrogen gas (6 mbar), and to perform the same measurement. As can be seen from Fig. 2, the TOF spectrum in this case shows a shift of a few ns corresponding to the energy loss of ions in cold hydrogen. Finally, in the third step the plasma is fired and further shift of the time spectrum is observed, due to the enhanced energy loss of heavy ions in ionized matter. The method described here provides a measurement of the energy loss relative to the vacuum calibration spectrum. The reliability of this method can be evaluated by a comparison of our energy-loss data for cold hydrogen gas to tabulated data,⁸ and we find an excellent agreement.

C. Energy-loss measurements

Since the investigation of interaction processes between hot ionized matter and beams of heavy ions is a rather new area of experimental research, we measured the energy loss in a plasma target systematically for a wide range

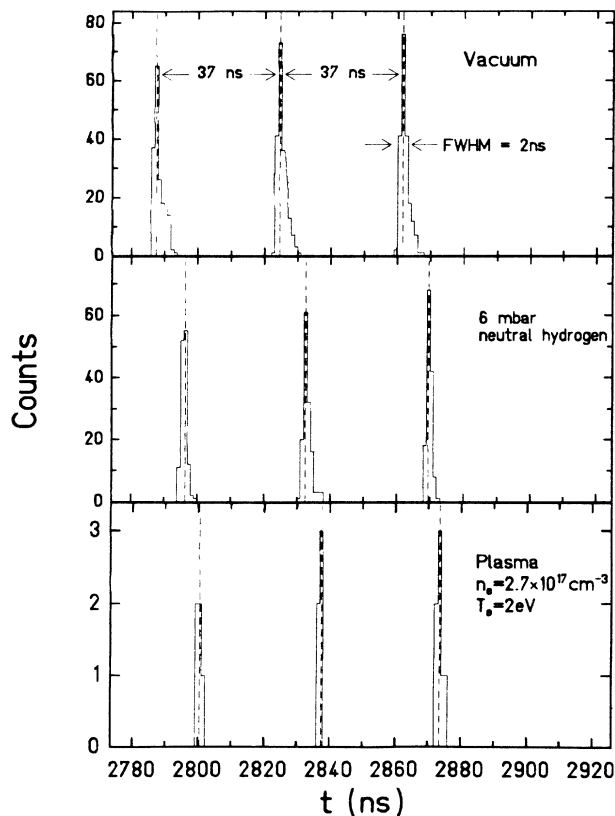


FIG. 2. Time-of-flight spectra for ^{74}Ge ions in different targets.

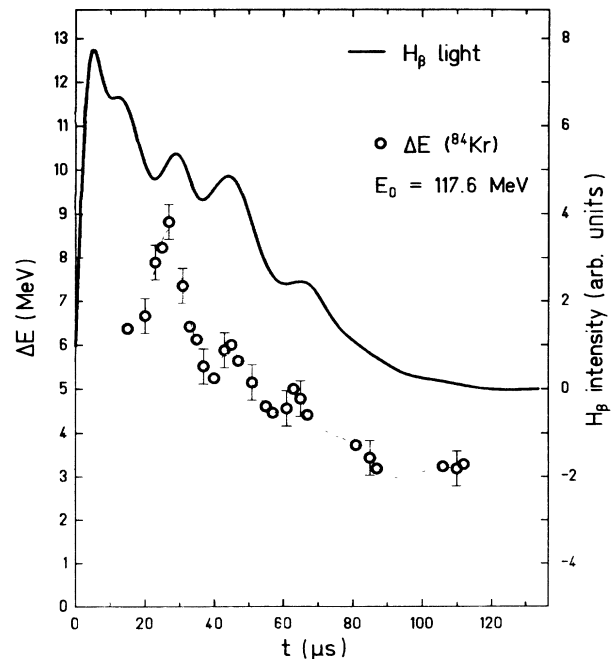


FIG. 3. Energy loss of ^{84}Kr ions in a hydrogen plasma, and the H_{β} -line emission from the discharge plasma.

of highly ionized heavy ions. A total of six different ion species was used in the experiment, including $^{40}\text{Ca}^{13+}$, $^{74}\text{Ge}^{18+}$, $^{84}\text{Kr}^{18+}$, $^{110}\text{Pd}^{26+}$, $^{208}\text{Pb}^{30+}$, and $^{238}\text{U}^{33+}$.

As a typical example we present in Fig. 3 the energy loss of krypton ions in a hydrogen plasma together with the H_β emission of the plasma as a function of time. Both curves show a similar oscillating behavior which is due to the oscillating current in the discharge circuit. Since the light output is proportional to square of the free-electron density (n_e) the oscillations also reflect the corresponding oscillations of the free-electron density.

Figure 4 shows the energy loss for three different ion species, ranging from ^{238}U to ^{40}Ca , i.e., from the heavy ion with the lowest mass number to the most heavy one used in our experiments. The energy-loss curves display a similar structure for all ions. Three maxima can be distinguished, with the first one being the most pronounced in all cases. The dashed lines in this figure always represent the energy loss of the respective ion species in cold hydrogen gas at a pressure of 6 mbar at room temperature, which are the initial conditions before a plasma shot.

During the first 10–15 μs after the plasma starts to emit light it is not accessible for measurements, since no beam pulses penetrate to the stop detector. For some of the ion species the same effect occurs in the region between 20 and 30 μs . From our diagnostic measurements we know that a pinch is formed during the first few microseconds and a very turbulent plasma is formed due to the instabilities arising from the pinch collapse. Parasitic magnetic fields induced by these phenomena deflect the

beam off axis, and prevent it from passing through the exit aperture of the plasma column. At other times we also observe an enhanced transmission through the plasma tube, which may also be explained by the focusing properties of high-current plasma discharges in z-pinch geometry.⁹

After 70 μs the measured energy loss drops below the value in the cold gas. The firing of the plasma causes a rarefaction wave, which reaches the axis by this time, and hence the density is lower than the initial one.

Comparing the maximum measured energy loss in the plasma to the value in neutral hydrogen, we find that the energy-loss enhancement varies between a factor of 2 and 2.6 from calcium to uranium. Finally, for a comparison of the experimental results with theoretical models, it is necessary to know the density of the target material as well as the energy loss.

D. Plasma diagnostics

The plasma parameter most relevant to the energy-loss measurement is the density of free electrons (n_e), whereas the variation of the electron temperature T_e is of minor influence as long as the ion velocity is large compared to the thermal velocity of the electrons. For the assessment of energy-loss contributions of free electrons relative to the stopping power of bound electrons, which are still present in nonionized hydrogen molecules and atoms, it is necessary to know the degree of ionization. Assuming local thermal equilibrium (LTE) in our plasma these three quantities are, however, strongly related to each other through the Saha equation. Thus with two of these parameters determined experimentally the third one can be calculated.

We used two different methods for plasma diagnostics: spectroscopy in a side-on spectroscopy and laser absorption measurements along the beam-plasma interaction axis. The plasma is optically thick along the axis for the H_β emission; therefore spectroscopic measurements had to be performed side on. With a system of a spectrometer coupled to a streak camera, we measured the light emission from the plasma resolved in wavelength and in time. The free-electron density n_e is determined from the half-width of the Stark-broadened H_β -line. From intensity ratios of the line radiation to the emission from the continuum the free-electron temperature T_e can be derived.¹⁰ The maximum values observed in our experiment are $n_e = 3 \times 10^{17} \text{ cm}^{-3}$ and $T_e = 2 \text{ eV}$ and occur at the same time when the maximum energy loss is measured. Evaluation of the Saha equation for these plasma parameters yields an almost fully ionized plasma.

A laser-absorption measurement provided a second independent method to diagnose the plasma parameters. The diagnostic measurement in this case was performed along the axis of the plasma column, collinear with the zone of interaction with the ion beam. The laser-absorption method to determine density and temperature of the plasma at the same time was first described in 1973 by Billman and Stallcop.¹¹ The transmitted fraction of the initial intensity I_0 depends strongly on the frequency of the laser light and on the plasma parameters n_e and T_e

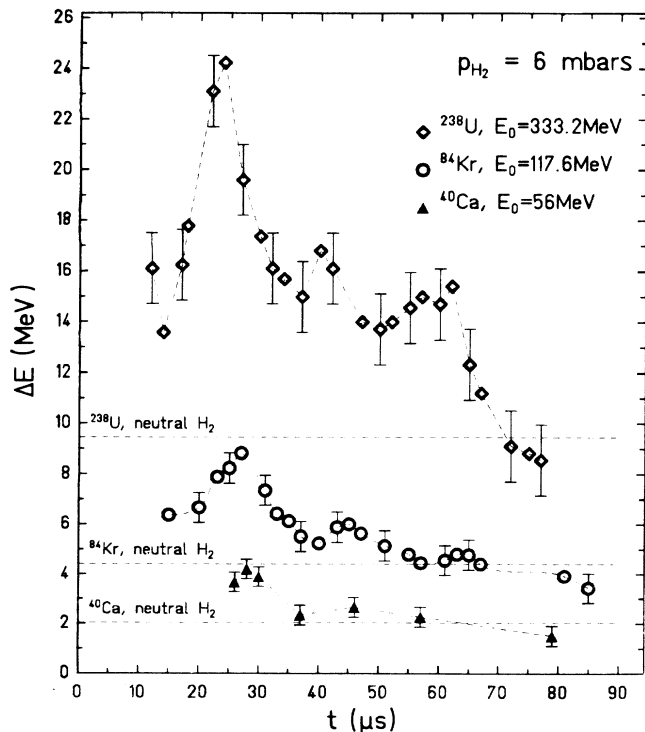


FIG. 4. Energy loss of different ion species (^{238}U , ^{84}Kr , ^{40}Ca) in the plasma target.

and can be written as

$$I = I_0 \exp[\kappa(\lambda, n_e, T_e)l],$$

where l is the length of the absorbing layer and κ the absorption coefficient. Hence, when the absorption coefficients of two different wavelengths are known, the parameters n_e and T_e can be determined. The two most intense lines of the argon-ion laser, used in this experiment, are $\lambda_1 = 488$ nm (blue) and $\lambda_2 = 514$ nm (green) and coincide nearly with the H_β -line and transitions in the continuum, respectively. The experimental setup to measure the absorption is shown in Fig. 5 with the emphasis on the diagnostic elements. We used an air-cooled argon-ion laser with an adjustable power output between 4 and 400 mW. After the passage through the plasma the beam was split in two components and each particular beam was passed through a wavelength filter of 488 and 514 nm, respectively. Lenses focused the beam components onto optical fibers to transmit the light to photodiodes which were especially sensitive in this wavelength regime. The photodiode signals were registered on a storage oscilloscope. With this method the transmitted laser-beam intensity was measured with high time resolution for both wavelengths during one single plasma ignition.

In Fig. 6 the development of the electron density n_e and temperature T_e as a function of the time after plasma ignition are shown. Again the oscillating behavior already observed in the light emission and the energy-loss curves can be noticed. The first maximum coincides with the moment of maximum energy loss. A temperature of 2 eV and a free-electron density of $n_e = 3 \times 10^{17} \text{ cm}^{-3}$ is measured. According to the Saha equation this corresponds to an ionization degree of 95% and the plasma can be regarded as fully ionized at this time.

The values for free-electron density and temperature shown in Fig. 6 indicate that the plasma is in LTE during the time interval relevant for the energy-loss measurement and therefore the degree of ionization can be determined from the Saha equation. In our evaluation we used tabulated values for the Saha equation.¹² The results for

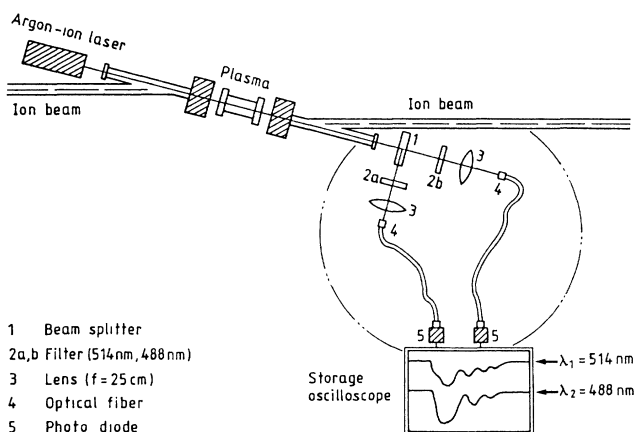


FIG. 5. Setup for the on-line plasma diagnostic.

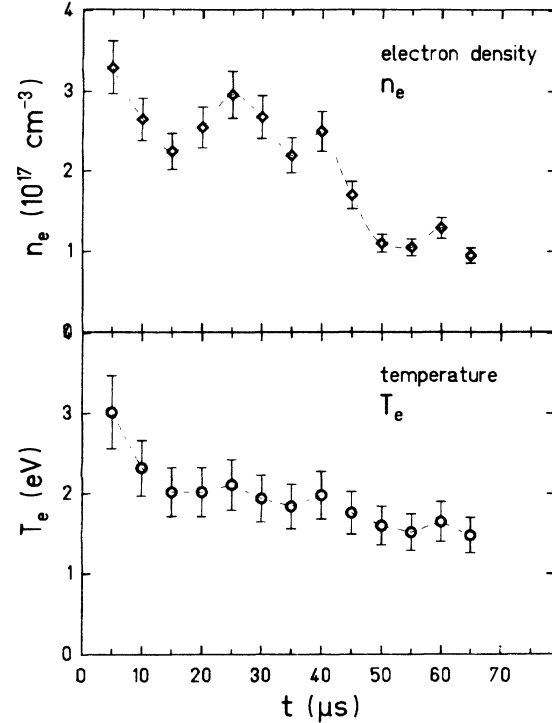


FIG. 6. Variation of plasma parameters, free-electron density n_e and temperature T_e , with time.

the degree of ionization were used to correct the measured energy loss in the plasma for the energy loss due to the amount of residual neutral hydrogen gas.

III. HEAVY ION STOPPING IN HOT IONIZED MATTER

The theoretical description of the energy loss of charged particles in cold, nonionized matter, is well established, well understood, and corroborated by a plethora of experimental data during a number of decades. This is, however, not the case for hot ionized matter and existing theories have not yet been verified by a large extent of experimental data.

When the ion velocity v is much larger than the thermal velocity of the free plasma electrons, an increase in stopping power is generally predicted,¹³⁻¹⁵ since the minimum energy transfer in a collision is no longer given by the average ionization potential \bar{I} but by the potential energy of the electrons in the Debye sphere. At high plasma temperatures, however, when the thermal electron velocity exceeds the projectile velocity, even a decrease of the stopping power combined with a large increase in range straggling is predicted.¹⁶

A. Enhanced stopping of ions in plasmas

In the energy regime considered in this experiment (1.4 MeV/u) the well-known Bethe formula without polarization correction and shell correction term describes the

energy loss of nonrelativistic charged particles in a hydrogen plasma ($Z_2 = 1$) in the following form:

$$-\left(\frac{dE}{dx}\right) = (Z_{\text{eff}} e \omega / v)^2 \ln \Lambda, \quad (1)$$

where Z_{eff} is the effective charge of the ion while it traverses the target, e is the electronic charge, and ω the plasma frequency, determined by the density of particles. For a cold target, where only bound electrons are present, the argument of the Coulomb logarithm Λ is given by

$$\Lambda_{\text{bound}} = 2mv^2 / \bar{I}. \quad (2)$$

This can be extended in a straightforward way to fully ionized material with free electrons using binary collision theory.¹⁷ The Coulomb logarithm in this case reads

$$\Lambda_{\text{free}} = 0.764v / b_{\text{min} \omega}. \quad (3)$$

The minimum impact parameter b_{min} depends on the velocity of the ion. Since the electronic mass m is negligible compared to the heavy-ion mass, the impact parameter is given by

$$b_{\text{min}} = \max(e^2 Z_{\text{eff}} / mv^2; \hbar / 2mv). \quad (4)$$

For the conditions of experiment ($v = 7.49\alpha c = 1.64 \times 10^9$ cm/s) b_{min} is always given by

$$b_{\text{min}} = e^2 Z_{\text{eff}} / mv^2, \quad (5)$$

due to the high charge state Z_{eff} of the incident ions, and thus we have

$$\Lambda_{\text{free}} = 0.764mv^3 / Z_{\text{eff}} e^2 \omega. \quad (6)$$

For comparison we list the Coulomb logarithm $\ln \Lambda_{\text{bound}}$ and $\ln \Lambda_{\text{free}}$ for cold and ionized hydrogen in columns 2 and 3 of Table I. The third column displays the ratio ($\ln \Lambda_{\text{free}} / \ln \Lambda_{\text{bound}}$), which is a factor of about 2, thus the enhancement in stopping power of a hydrogen plasma as compared to cold hydrogen gas is also of the order of a factor of 2, for all heavy ions.

B. Model description of the heavy-ion effective charge state

The charge state of heavy ions passing through matter is fluctuating rapidly, due to ionization and electron-capture processes. A dynamic equilibrium of these pro-

cesses finally determines the effective charge state Z_{eff} which is one key parameter in Eq. (1), and it turns out to be a function of the target thickness x , the ion velocity v , and the temperature T of the target material¹⁸ [$Z_{\text{eff}} = Z_{\text{eff}}(x, v, T)$]. For a complete evaluation of the energy-loss equation (1), the x dependence of Z_{eff} has to be analyzed. A detailed treatment of this problem is found, e.g., in Ref. 19. For our purpose we developed a Monte Carlo code to track the development of the heavy-ion effective charge state, as the projectile traverses the plasma target, and used the results as an input to an energy-loss calculation. In this code we treated ionization processes due to collisions of the heavy-ion projectile with bound and free target electrons, and target nuclei in the framework of the binary encounter model of Gryzinski.²⁰

The dominant electron-capture process in our experiment was recombination by capture of bound electrons, and in the case of the fully ionized plasma target, radiative electron capture (REC).

For highly charged ions such as U^{33+} , which we regard as our standard example, electron-capture processes occur to states with high principal quantum numbers, which are difficult to treat. The Oppenheimer-Brinkmann-Kramers (OBK) approximation provides, however, a simple method to describe these processes. Since in this experiment we are dealing with a hydrogen target, we used the Nilolaev formula²¹ for K-shell electron transfer to a projectile state with principal quantum number n and performed a summation over all possible n states up to the convergence limit. The resulting cross sections are known to overestimate experimental data,²² and we therefore applied the Chan-Eichler scaling factor to the OBK cross section.²³

An empirical scaling rule for the electron-capture cross section into highly charged ions described by Schlachter and co-workers²⁴ represents our data equally well and due to its parametrization is especially suited to be used in a computer code.

In Fig. 7 we present the development of the charge state of uranium ions in a hydrogen target as a function

TABLE I. Coulomb logarithm in cold (Λ_{bound}) and fully ionized (Λ_{free}) hydrogen with $n_e = 3 \times 10^{17}$ cm⁻³ and $v = 7.49\alpha c = 1.64 \times 10^9$ cm/s.

Ion	$\ln \Lambda_{\text{bound}}$	$\ln \Lambda_{\text{free}}$	$\ln \Lambda_{\text{free}} / \ln \Lambda_{\text{bound}}$
Ca ¹³⁺	5.42	10.42	1.92
Ge ¹⁸⁺	5.42	10.09	1.86
Kr ¹⁸⁺	5.42	10.09	1.86
Pd ²⁶⁺	5.42	9.72	1.79
Pb ³⁰⁺	5.42	9.58	1.77
U ³³⁺	5.42	9.48	1.75

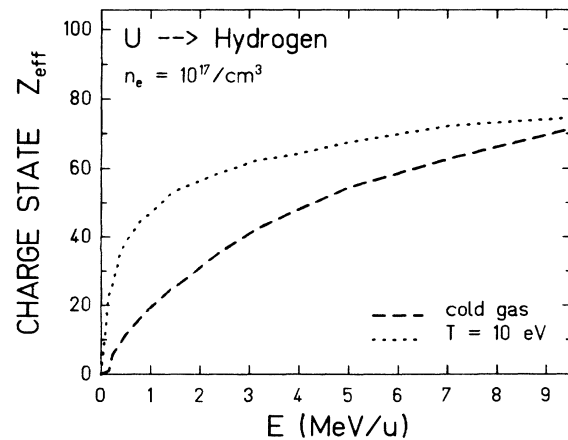


FIG. 7. Effective charge of U ions vs energy.

of the ion energy. The dotted curve is our calculation for a fully ionized hydrogen plasma target at a temperature of 10 eV. The dashed curve is the semiempirical Betz formula²⁵ which describes the equilibrium charge state of ions in cold matter.

At very high ion energy both curves will approach the charge state $92+$ of completely stripped uranium. With decreasing energy the charge state in cold hydrogen gas is a smoothly varying function of ion energy, whereas in the case of an ionized plasma target, the charge state tends to stay at a high level over a large range of energy, and to drop steeply at low energies. In the energy range between 1 and 2 MeV/u the difference in both cases is most pronounced. Therefore we choose the energy of 1.4 MeV/u for this experiment to be most sensitive on charge state effects for the slowing down of energetic, highly charged ions in a plasma target.

The development of the ion charge state during the passage of the target depends strongly on the target state. In Fig. 8 the following scenario is considered. Uranium ions of charge state $33+$ impinge on the hydrogen gas target at an energy of 1.4 MeV/u. This charge state is well above the equilibrium charge state ($28+$). Therefore electron-capture processes from bound target electrons will decrease the ion charge state rapidly while it traverses the cold hydrogen gas. In a plasma target, however, electron-capture processes are reduced, since only free electrons are present. Ionization due to collisions with target nuclei is the dominant ionization mechanism and does not change significantly with a rise of temperature in the few-eV regime. Therefore ionization rates prevail over electron-capture rates and the charge state tends to even increase further while the ion moves through the target. It is an important feature of this experiment that the initial charge state of the ions was always chosen to be 10–15% above the equilibrium charge state in cold gas. Therefore, even in a comparatively low-density target ($n_e = 10^{17} \text{ cm}^{-3}$) the effective charge of the ions starts to develop in opposite directions, depending on whether the target is cold hydrogen gas or a fully ionized plasma.

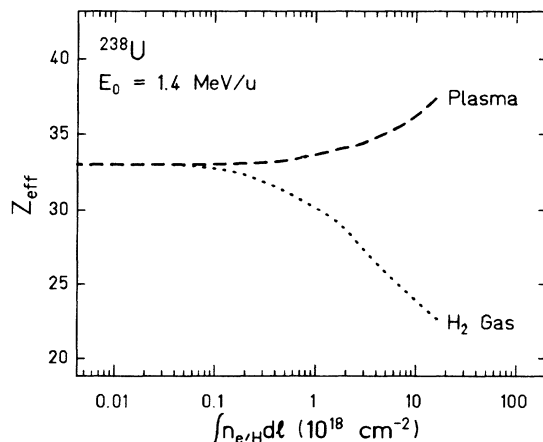


FIG. 8. Effective charge state of ^{238}U ions during target passage.

C. Comparison of experiment results and theory

With the development of the code mentioned in the preceding section, which takes into account the important features of charge-changing cross sections and energy-loss mechanisms in cold and ionized matter, we had the proper tools at hand to compare the model predictions with experimental data.

Figures 9 and 10 illustrate this comparison. In Fig. 9 the experimental results for the energy loss of ^{238}U ions in the hydrogen plasma and in neutral hydrogen gas as a function of target density are shown together with four theoretical predictions calculated by the code described in Sec. III B.

The dashed lines were derived under the assumption that the original charge state of the incident uranium ion ($33+$) is preserved, which is valid as a first approach but not very realistic. The solid lines, on the other hand, were calculated considering the variation of the effective charge state of the ions, which is a function of the target thickness traversed by the heavy ion, as was shown already in Fig. 8.

For cold hydrogen gas (lower solid line) standard stopping theory agrees quite well with the experimental results when the variation of Z_{eff} inside the target is taken into account properly. Moreover, we like to emphasize that the data point at the lowest target density is right on top of the energy-loss predictions from Northcliffe and Schilling⁸ data tables. The overall agreement with these semiempirical predictions is within 10–15% for all our measurements in cold hydrogen gas. At higher target densities the experimental data tend to be above the theoretical prediction. This behavior is due to the OBK electron-capture cross section which has the tendency to exceed experimental data that have been obtained at the 1.4-MeV/u experimental area at GSI earlier.²⁶

Due to the difficult measurement of the plasma parameter along with the energy-loss measurement, and the reproducibility of the plasma conditions from shot to shot, the measured energy-loss data in the hydrogen plas-

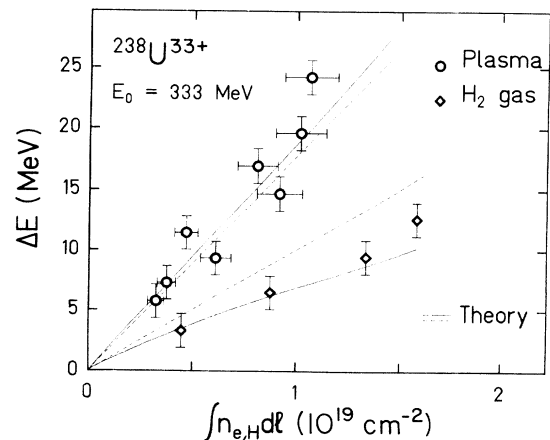


FIG. 9. Comparison of experimental data and stopping theory for ^{238}U ions.

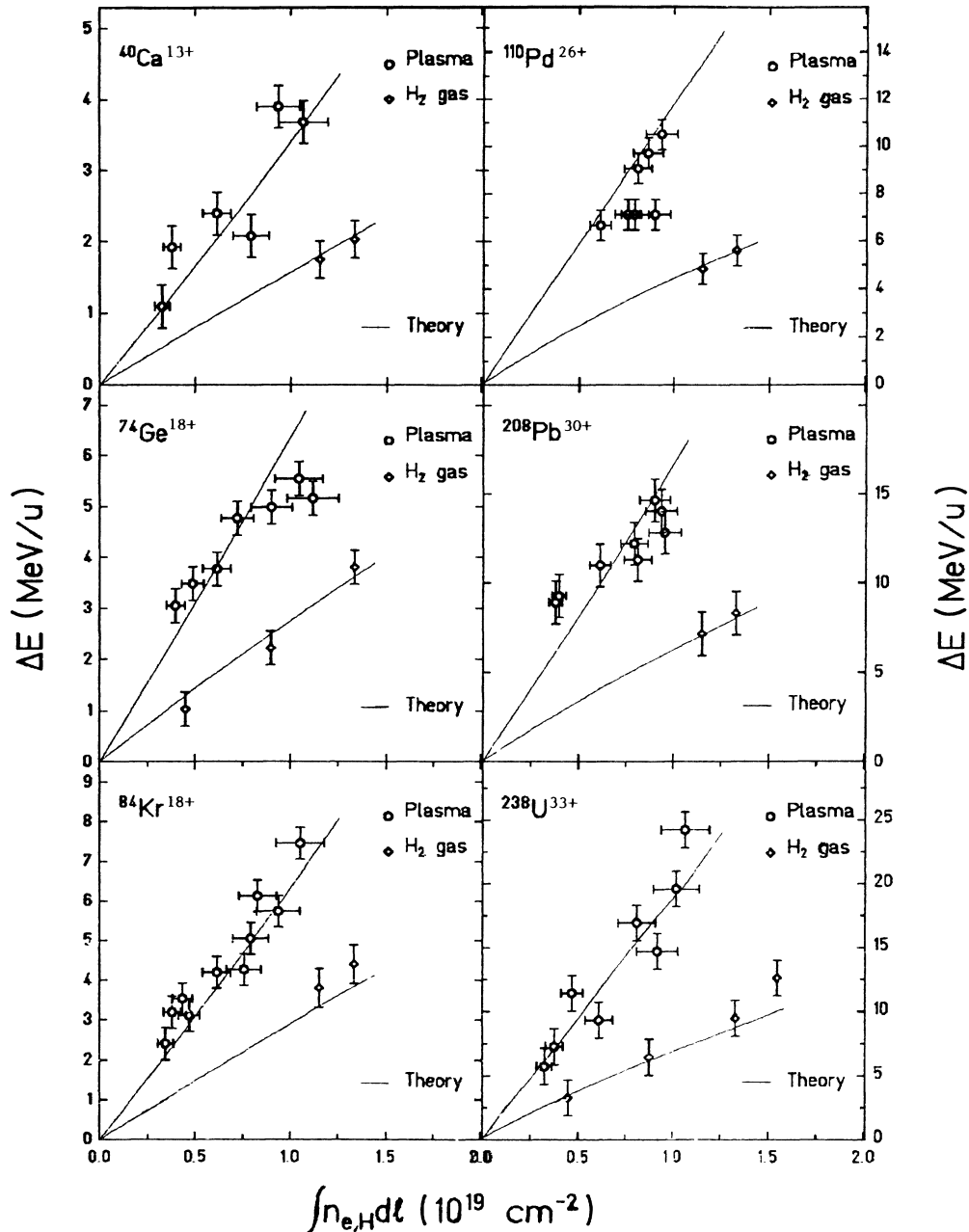


FIG. 10. Energy-loss data and theory for different ion species.

ma exhibit some statistical distribution around the calculated curves (upper dashed and solid lines in Fig. 9). The differences in energy loss due to a variation of the charge state in the ionized material are too small to be experimentally distinguished from a constant- Z_{eff} behavior, for densities obtained in this experiment. But the enhanced energy loss in fully ionized matter as compared to the energy loss in cold matter is clearly demonstrated beyond experimental uncertainties.

In Fig. 10 we extend the comparison between experiment and theory further to include all our measured data. In this figure only those calculations are shown where the variation of Z_{eff} with increasing target thickness is considered. For all six ion species used in this experiment

the enhanced stopping power of ionized matter is observed. The theoretical model is in good agreement with the experimental results. The increase in stopping power varies from a factor of 2 for the heavy ion with the smallest mass number in our experiment (^{40}Ca) to 2.6 for uranium. It is tempting to attribute this increase to the fact that a variation of the effective charge state Z_{eff} is more effective to influence the total energy loss for higher atomic numbers of the projectile.

IV. CONCLUSIONS

With this experiment it has been possible for the first time to measure the energy loss of a wide range of heavy

ions in a plasma environment and confirm that ionized matter has indeed a different stopping power than cold matter. The experimental results are in good agreement with the theoretical expectations and confirm the theoretical models based on the Bethe-Bohr-Bloch stopping theory.

In this experiment we were able to establish a stopping power enhancement of a factor of 2 and higher. Indications for this behavior have been reported earlier for light ions^{2,3,27,28} and for the case of uranium in the early phase of our experiment.²⁹ Furthermore from the survey of a wide range of heavy-ion species, this experiment indicates an increase of the projectile charge state Z_{eff} while the

ion traverses the plasma. This effect adds to the effect of an enhanced stopping power of ionized matter due to the variation of the Coulomb logarithm.

The aim of the experimental research in this field is now to extend the measurements into the regime of even higher-density plasmas, and to probe the plasma with a more energetic ion beam.

ACKNOWLEDGMENTS

This work was funded by Bundesministerium für Forschung und Technologie (Bonn, West Germany).

*Permanent address: Gesellschaft für Schwerionenforschung Darmstadt m.b.H., Postfach 110552, 6100, Darmstadt, West Germany.

¹D. H. H. Hoffmann, J. Meyer-ter-Vehn, R. W. Müller, I. Hoffmann, R. Bock, and R. Arnold, Nucl. Instrum. Methods A **278**, 44 (1989).

²F. C. Young, D. Mosher, S. J. Stephanakis, S. A. Goldstein, and T. A. Mehlhorn, Phys. Rev. Lett. **49**, 549 (1982).

³P. M. Evans, A. P. Fewes, and W. T. Toner, Laser Part. Beams **6**, 353 (1988).

⁴R. Bimbot, S. Della-Negra, M. Dumail, D. Gardés, M. F. Rivet, C. Fleurier, A. Sanba, B. Dumax, D. H. H. Hoffmann, K. Weyrich, J. Jacoby, H. Wahl, C. Deutsch, and G. Maynard, Laser Interact. **8**, 665 (1988).

⁵D. H. H. Hoffmann, J. Jacoby, H. Wahl, K. Weyrich, R. Noll, C. R. Haas, and B. Weikl, in *Heavy Ion Inertial Fusion, Washington, D.C., 1986*, Proceedings of the International Symposium on Heavy Ion Fusion, AIP Conf. Proc. No. 152, edited by Martin Reiser, Terry Godlove, and Roger Bangertner (AIP, New York, 1986).

⁶E. Festa and R. Sellem, Nucl. Instrum. Methods **188**, 99 (1981).

⁷E. Festa, R. Sellem, and L. Tassan-Got, Nucl. Instrum. Methods A **234**, 305 (1985).

⁸L. C. Northcliffe and R. F. Schilling, Nucl. Data Tables A **7**, 233 (1970).

⁹D. Gardes, R. Bimbot, S. Della Negra, M. Dumail, B. Kubica, A. Richard, M. F. Rivet, A. Servajean, C. Fleurier, A. Sanba, C. Deutsch, G. Maynard, D. H. H. Hoffmann, K. Weyrich, and H. Wahl, Europhys. Lett. **8**, 701 (1988).

¹⁰W. Lochte-Holtgreven, *Plasma Diagnostics* (North-Holland, Amsterdam, 1968), Chap. 3.

¹¹K. W. Billman and J. R. Stallcop, Appl. Phys. Lett. **22**, 565 (1973).

¹²A. Eberhagen and W. Lünow, Max-Planck-Institute für Plasmaphysik (MPIPP) Report No. IPP/1/23, Garching, 1964 (unpublished); IPP Report No. IPP/6/20, Garching,

1964 (unpublished).

¹³E. Nardi, E. Peleg, and Z. Zinamon, Phys. Fluids **21**, 574 (1978).

¹⁴T. A. Mehlhorn, J. Appl. Phys. **52**, 6522 (1981).

¹⁵C. Deutsch, P. Fromy, X. Garbet, and G. Maynard, Fus. Technol. **13**, 362 (1988).

¹⁶M. M. Basko, Fiz. Plazmy **10**, 1195 (1984) [Sov. J. Plasma Phys. **10**, 689 (1984)].

¹⁷J. D. Jackson, *Classical Electrodynamics* (Wiley, New York, 1975), Chap. 13.

¹⁸E. Nardi and Z. Zinamon, Phys. Rev. Lett. **49**, 1251 (1982).

¹⁹T. Peter, Ph.D. thesis, University of TU-München, 1985 (unpublished); MPQ Report No. MPQ 105, 1985 (unpublished).

²⁰M. Gryzinski, Phys. Rev. A **138**, 305 (1965).

²¹V. Nikolaev, Zh. Eksp. Teor. Fiz. **51**, 1263 (1966).

²²A. M. Halpern and J. Law, Phys. Rev. **31**, 4 (1973).

²³F. T. Chan and J. Eichler, Phys. Rev. Lett. **42**, 58 (1979).

²⁴A. S. Schlachter, J. W. Stearns, W. G. Graham, K. H. Berkner, R. V. Pyle, and J. A. Tanis, Phys. Rev. A **27**, 3372 (1983).

²⁵H. D. Betz, G. Horting, E. Leischner, Ch. Schmelzer, B. Stadler, and J. Weikrauch, Phys. Lett. **22**, 643 (1966).

²⁶W. Erb, Gesellschaft für Schwerionenforschung—Darmstadt Report No. GSI-P-7-78, 1978 (unpublished).

²⁷J. N. Olson and T. A. Mehlhorn, J. Appl. Phys. **58**, 1251 (1985).

²⁸H. Bluhm, B. Goel, P. Hoppe, H. U. Karow, and D. Rush, in *Proceedings of the 7th International Conference on High-Power Particle Beams, Karlsruhe, 1988*, edited by W. Bauer and W. Schmidt (Kernforschungszentrum, GmbH, Karlsruhe, 1988), p. 381.

²⁹D. H. H. Hoffmann, K. Weyrich, H. Wahl, Th. Peter, J. Meyer-ter-Vehn, J. Jacoby, R. Bimbot, D. Gardes, M. F. Rivet, M. Dumail, C. Fleurier, A. Sanba, C. Deutsch, G. Maynard, R. Noll, R. Haas, R. Arnold, and S. Maurmann, Z. Phys. A **30**, 339 (1988).